Composites Part C: Open Access 15 (2024) 100520

Contents lists available at ScienceDirect

Composites Part C: Open Access

journal homepage: www.sciencedirect.com/journal/composites-part-c-open-access

Bioinspired surface modification of mussel shells and their application as a biogenic filler in polypropylene composites

Jing Xu [a,b,*], Michael R. Mucalo [a,*], Kim L. Pickering [b]

[a] School of Science, The University of Waikato, Hamilton, New Zealand
[b] School of Engineering, The University of Waikato, Hamilton, New Zealand

ARTICLE INFO

Keywords:
PP composite
Mussel shell
Surface modification
Interfacial adhesion

ABSTRACT

This study explores the potential of mussel shells (MS) as biogenic fillers in polymer composites. The chemical composition and crystal structures of MS were characterised. To improve MS filler dispersion and adhesion within a polypropylene (PP) matrix, three surface modification methods were evaluated: polydopamine (PDA) coating, maleic anhydride-grafted polypropylene (MAPP) modification, and PDA/MAPP co-modification. The PDA coating, inspired by the adhesive properties of mussel foot proteins, successfully functionalized the MS surface, as confirmed by X-ray photoelectron spectroscopy (XPS). Thermodynamic analysis, based on contact angle measurements, revealed that MAPP and PDA/MAPP modifications reduced surface energies and potential energy differences. These changes enhanced filler dispersion and interfacial bonding by increasing hydrophobicity and reducing agglomeration in the PP matrix. Consequently, PP composites with 20% PDA/MAPP-modified MS fillers exhibited a 2.9% increase in tensile strength and a 7.5% increase in flexural strength compared to neat PP. Scanning electron microscopy (SEM) also showed reduced filler-matrix debonding and fewer voids. The proposed mechanism attributes these macroscopic property enhancements to the ability of the PDA coating to facilitate chemical and hydrogen bonding between MS fillers and MAPP.

1. Introduction

Calcium carbonate ($CaCO_3$) is commonly used as a mineral filler in polymer composites due to its natural abundance, cost-effectiveness, and the ability to improve mechanical properties [1]. Limestone is the most prevalent natural form of calcium carbonate and is found in sedimentary rocks. Alternatively, marine organism shells can serve as a sustainable source of biogenic calcium carbonate, which can be used to produce biomaterials by volatilizing waste. Mollusc production has consistently increased worldwide. According to the Fishery and Aquaculture Statistics Yearbook 2021, mussel aquaculture production increased from less than 0.8 million tonnes per year in the 1980s to over 2 million tonnes in 2021 [2]. Growing mussel production results in significant shell waste, as shells account for 70–80% of the mussel's weight. [3-5]. Generally, waste mollusc shells are discarded because there is no established market for them, leading to issues such as inappropriate land use, unpleasant odors, and unsightly landscapes [1]. Direct disposal of shell waste into the sea has been prohibited in countries such as New Zealand [6], and shell waste is categorized as special waste under European regulations. The high disposal cost, approximately 25 Euros per kilogram, imposes a significant economic burden on the related industries [5].

Mollusc shells, including those from mussels, oysters, scallops, clams, and cockles, consist of over 95% calcium carbonate and 3–5% organic material [1,7]. This high calcium carbonate content makes shell waste a cost-effective source of biogenic calcium carbonate. Mussel shells, in particular, are abundant by-products of the seafood industry and mussel farming, further highlighting their potential as a low-cost resource. Consequently, these shells have been explored as valuable fillers for various polymers, including polyethylene (PE) [8,9], polypropylene (PP) [5,10-13], polylactic acid (PLA) [14-16], and polyurethane (PU) [17]. Incorporating shell fillers into polymers not only helps reduce product costs and improve processing aspects, such as mold release, but also enhances mechanical properties. For instance, shell fillers can increase rigidity in PP [18], compressive strength and wear resistance of Poly (Methyl methacrylate) [19], and tensile strength in PLA [14], while also improving other material properties such as fire retardancy [20,21]. This demonstrates the potential to valorise shell waste into valuable, bio-renewable products derived from natural sources.

Calcium carbonate exists in three crystalline forms: vaterite,

* Corresponding authors.
E-mail addresses: jx111@students.waikato.nz.ac (J. Xu), michael.mucalo@waikato.ac.nz (M.R. Mucalo).

https://doi.org/10.1016/j.jcomc.2024.100520

Available online 28 September 2024

aragonite, and calcite. The three polymorphs of calcium carbonate are distinct in properties such as solubility, thermodynamic stability, morphology, and average crystal size [22]. From a thermodynamic perspective, vaterite is the least stable, while calcite and aragonite are relatively stable under ambient conditions [23]. Geogenic $CaCO_3$, such as that derived from limestone, predominantly consists of calcite. In contrast, the biomineralization process regulated by organic matter in mollusc shells results in the formation of both aragonite and calcite [24,25].

It is well recognized that the superior properties of polymer composites depend on effective particle dispersion, interfacial compatibility, and strong filler-matrix adhesion, all of which are influenced by the surface treatment of the filler particles and the production methods used [26]. However, incorporating $CaCO_3$ fillers into hydrophobic polymers presents significant challenges due to their hydrophilic nature and high surface energy. The fillers often agglomerate due to incompatibility with the polymer matrix and result in inadequate dispersion. This leads to the creation of weak points within the polymer matrix and weakens the filler-matrix interfacial adhesion [27]. Consequently, the mechanical properties and applicability of the resulting composites are often compromised.

Surface modification of calcium carbonate fillers is essential for mitigating these issues and improving compatibility with polymers, particularly polypropylene (PP) and polyethylene (PE), which inherently have low polarity and surface energy (approximately 35 mJ/m^2) [13]. Low-molecular-weight reagents, such as monocarboxylic acids and their salts [28,29], as well as silane and titanate coupling agents [27,30], are commonly used to enhance the compatibility and dispersion of calcium carbonate fillers in hydrophobic polymers. Grafted polyolefins, like maleic anhydride-grafted polypropylene (MAPP), are recognized for effectively improving the adhesion and dispersion of fillers within polymer matrices [31].

Similarly, surface modification methods have been applied to shell-derived calcium carbonate to enhance its compatibility with polymers. Pimelic acid-modified scallop shells have been reported to exhibit improved dispersion and enhanced interfacial adhesion with the polypropylene matrix. Scanning electron microscopy (SEM) analysis of the fracture surface of the filled PP composite revealed that the shell powder was well-coated with organic pimelic acid, improving its compatibility with the nonpolar PP matrix. Consequently, the addition of pimelic acid-modified shells did not significantly reduce the tensile and flexural properties of the resulting PP composites [12]. Furfural-modified clam shell was obtained at a weight ratio of 1:5 using a ball milling method. These modified shell fillers act as a heterogeneous nucleating agent for the PP matrix, improving the impact strength of the filled PP composite compared to neat PP [32]. Previous studies have reported that although the incorporation of a 5% titanate coupling agent did not significantly improve the interfacial interaction between the modified shell-waste particles and the HDPE matrix, it did enhance the thermal properties of the resulting composite [8]. Liu et al. reported an organic surface modification method where pearl shell powders (PSP) were treated with Direct Red 28 (DR 28) dye. Concurrently, maleic anhydride-grafted polyethylene (PE-g-MAH) was introduced into the polyethylene (PE) matrix, imparting hydrophilic properties to it. This approach facilitated effective filler dispersion and enhanced interfacial adhesion due to the polar interactions between the maleic anhydride groups and the dye-modified PSP [33]. Achatina fulica shell-derived $CaCO_3$ was synthesized via mechanochemical processes, involving wet milling of coarse (< 50 μm) shell particles using different solvents: water, methanol, ethylene glycol, and ethanol. Nano-$CaCO_3$ synthesized using ethanol and methanol was added as fillers in epoxy, resulting in a 22.42% and 21.34% increase in tensile strength compared to neat epoxy. This enhancement is credited to the well-dispersed particles within the polymer, confirmed by transmission electron microscopy (TEM) analysis. However, a drawback of this method is the prolonged milling period required for shell processing [34].

Facile surface modification methods for shell fillers are still limited in scope. Challenges such as the complexity of composite preparation, low filling content, and limited enhancement efficiency arising from the use of shell powders as fillers remain unresolved [34]. To increase the utilization of shell fillers, it is crucial to achieve optimal compatibility with polymers and enhance their filling content. Such improvements not only optimize the performance of the fillers but also facilitate the sustainable and value-added utilization of these by-products.

Mussels can adhere to diverse surface compositions, including both inorganic and organic substrates, even materials traditionally resistant to adhesion like poly(tetrafluoroethylene) (PTFE) [35,36]. The strong adhesion originates from mussel foot proteins, which contain a special catecholic residue, 3,4-dihydroxyphenylalanine (DOPA). Dopamine, a key derivative of the DOPA structure, can form a hydrophilic polymer, polydopamine, through self-polymerization in alkaline conditions. This one-step method was first adopted by Lee *et al.* in 2007 [36]. Polydopamine (PDA) has been extensively studied in materials science, primarily due to its abundant functional groups. These functional groups enable PDA to serve as an adaptable platform for precise functionalization, which is crucial for various applications. Furthermore, PDA film can be formed on the surface of various materials, including metals, inorganic materials, and nonmetals, as well as polymers [37].

PDA coating has been demonstrated to effectively enhance filler-matrix adhesion with various fillers such as polyethylene fibre [38], nanoclays [39], and carbon fibres [40]. This improvement can be attributed to the unique chemistry and reactive functional groups of PDA. For instance, after PDA modification, $BaTiO_3$ nanoparticles and nanofibres can be homogeneously dispersed within the epoxy matrix, resulting in nanocomposites of higher quality and better breakdown strength [41]. This is due to the enhanced bonding interactions between the polymer and the surface-modified $BaTiO_3$. PDA coating was also employed for the surface modification of four ceramic nanofibres: $Na_2Ti_3O_7$, TiO_2, $BaTiO_3$, and $SrTiO_3$. For all, the modified nanofillers were found to demonstrate homogeneous dispersion within the polyvinylidene difluoride (PVDF) matrix [42]. Yuan et al. observed that the surface average roughness (Ra) of carbon fibre (CF) increased from 35 nm to 47 nm after polydopamine (PDA) coating. This increase in surface roughness is expected to enhance the physical interlocking between the fibre and the matrix. When combined with maleic anhydride-grafted polypropylene (MAPP), polypropylene composites incorporating 30% PDA-coated carbon fibre exhibit significantly improved mechanical properties, including a 105% increase in flexural strength, a 48% increase in flexural modulus, and a 223% increase in impact strength compared to PP composites with uncoated CFs. The PDA coating improves the wettability of the fibre, and it is argued that the amine groups from PDA form chemical bonds with the maleic anhydride groups. Both of these factors contribute to the enhanced mechanical properties [40].

This study aims to investigate the use of local shell waste, specifically the shells of New Zealand green-lipped mussels (Perna canaliculus), as a source of biogenic calcium carbonate. The potential of these native mussel shells as alternative fillers for calcium carbonate in polypropylene composites was evaluated by analyzing their chemical composition, particle size distribution, and surface properties.

Research on utilizing waste shells as biofillers for polymer composites remains limited, particularly regarding a comprehensive understanding of the surface properties of shell fillers and their impact on the interfacial adhesion between filler and matrix. This study applies three surface modification techniques to the mussel shells: polydopamine (PDA) coating, maleic anhydride-grafted polypropylene (MAPP) modification, and a combination of PDA and MAPP modification. To evaluate the surface properties of both unmodified and surface-modified mussel shell fillers, two empirical models—the Fowkes and Owens-Wendt models—were used based on contact angle measurements. This thermodynamic analysis aimed to determine their hydrophobicity levels and predict tendencies for filler agglomeration and re-agglomeration upon incorporation into PP. Moreover, the impact of surface modification on

the macroscopic properties of PP composites filled with different mussel shell fillers was assessed by examining the mechanical properties and fracture morphology of these composites. Mechanisms explaining the efficacy of MAPP and PDA/MAPP co-modification on mussel shell fillers were proposed based on thermodynamic analysis and macroscopic properties.

2. Materials and methods

2.1. Materials

Tris(hydroxymethyl)-aminomethane (TRIS, 99 %), dopamine hydrochloride (DOPA-HCl, 98 %), hydrochloric acid (HCl, 37%), diiodomethane (DIM, 99 %), commercial calcium carbonate (CC, >98%), MAPP with a molecular weight (Mn) of 8000 and a melting point of 140 °C, supplied by Sigma-Aldrich and used as received. Potassium bromide (IR spectroscopy grade) was purchased from Merck. Polypropylene (Moplen EP548S), purchased from LyondellBasell, has a melt flow index of 44 g/10 min and a density of 0.9 g/cm^3. Mussel shells were generously provided by North Island Mussels Ltd, where they were initially processed into 5-10 cm pieces at the factory. Subsequently, the shells underwent a washing process using tap water to remove impurities. To ensure the elimination of bacteria and moisture, the cleaned shells was dried in an oven at 135 °C for 0.5 h followed by further drying at 100 ± 5 °C for 12 h. The dried mussel shells (MS) were then subjected to dry milling in a planetary ball mill (model PM 100, Retsch, Germany) for 45 min, followed by sieving to obtain particles smaller than 200 μm.

2.2. Methods

2.2.1. Preparation of polydopamine coated mussel shells (PDA-MS)

2 L of Tris–HCl (20 mM) buffer solution was prepared and pH adjusted to 8.5 with 1 M HCl, and heated to 45 °C. With vigorous stirring at 600 rpm, 20 g of mussel shell particles (10 g/L) and 4 g of dopamine (2 g/L)) were added. The suspension was then stirred at 45 °C for 24 h to facilitate the self-polymerization reaction (colour changed over the period of 24 h as shown in Fig. 1). Treated mussel shell particles were filtered, washed with deionized water until the pH of the filtrate reached 7, and dried in an oven at about 105 °C for 12 h.

The self-polymerization of dopamine into polydopamine was shown in Fig. 2. Due to the structural complexity of polydopamine, the illustrated structure of polydopamine was adopted from literature [35].

2.2.2. Preparation of MAPP modified mussel shell, PDA and MAPP co-modified mussel shell

MAPP-modified mussel shells (MAPP-MS) were prepared by dry-milling MAPP together with mussel shells in a planetary ball mill for 45 min at a weight ratio of MAPP to mussel shells of 3:5, followed by sieving to obtain particles smaller than 200 μm. Similarly, polydopamine and MAPP co-modified mussel shells (PDA/MAPP-MS) were prepared using the same procedure, combining MAPP and polydopamine-modified mussel shells at a weight ratio of MAPP to PDA-MS of 3:5. Before milling, MAPP, mussel shell powders, PDA-MS powders were oven dried for 1 h at 100 ± 5 °C.The schematic illustration can be found in Fig. 3, surface modification section.

2.2.3. Preparation of polypropylene (PP) composites

Firstly, master batches were prepared for PP composites by melt-mixing PP with fillers such as MS, MAPP-MS, and PDA/MAPP-MS, respectively. Compounding occurred using a custom sigma blade melt compounder at 185 °C and a mixing speed of 30 rpm. In the next stage, PP or PP composites were extruded with a Labtech LTE-20–44 Twin-screw extruder at a screw rotation rate of 20 rpm and barrel temperatures between 160 and 185 °C. Additional polypropylene was introduced during this phase to adjust the filler content in the composite to either 5 wt% or 20 wt%, while maintaining the MAPP content at 3 wt%. The extruded materials were then pelletized and dried overnight in an oven set at about 105 °C.

Tensile testing samples were produced by injection molding using a BOY 35A injection molding machine. Injection processing parameters included temperatures ranging from 165 to 190 °C, an injection time of 0.5 s, and cooling times of 30 s. The formulations of PP composites were detailed in Table 1.

2.3. Characterization

2.3.1. Fourier transform infrared (FTIR) spectroscopy

Infrared spectra were acquired using a Perkin Elmer® Spectrum 100 FTIR spectrometer in transmission mode. Samples were prepared via KBr pellet pressing. Spectra were recorded in the range of 4000 - 400 cm^{-1} with 10 scans at 4 cm^{-1} resolution.

2.3.2. Solid-state nuclear magnetic resonance (SS-NMR) spectroscopy

The acquisition of the ^{13}C MAS NMR spectra required was done using a JEOL 600 MHz NMR spectrometer equipped with a broadband solids probe with magic angle spinning. Powder samples were packed into 3.2 mm zirconia rotors with PTFE caps and spun at a frequency ν_{MAS} =10 kHz. Spectra were recorded at a frequency of 150.9 MHz for 13C using a single pulse with decoupling, a relaxation delay of 180 s, and a temperature of 20–21 °C. The fully decoupled free induction decay (FID) was accumulated over 172 to 640 scans and Fourier-transformed with phase and baseline corrections to obtain the line spectrum. Spectra were integrated using Delta™ Software v5.3.3 and chemical shifts were referenced to a separately acquired ^{13}C ^{1}H cross polarised spectrum of solid adamantane spun at 5 kHz.

2.3.3. X-ray diffraction (XRD) analysis

XRD analysis was carried out on commercial $CaCO_3$, pristine mussel shell powder and polydopamine coated mussel shell powder using a Panalytical Empyrean X-ray diffractometer with CuKα radiation. Powder samples were carefully packed and pressed into disks using steel holders. Subsequently, samples were scanned between 20–60 ° (2θ) using steps of 0.026 ° at a speed of 1 °/min.

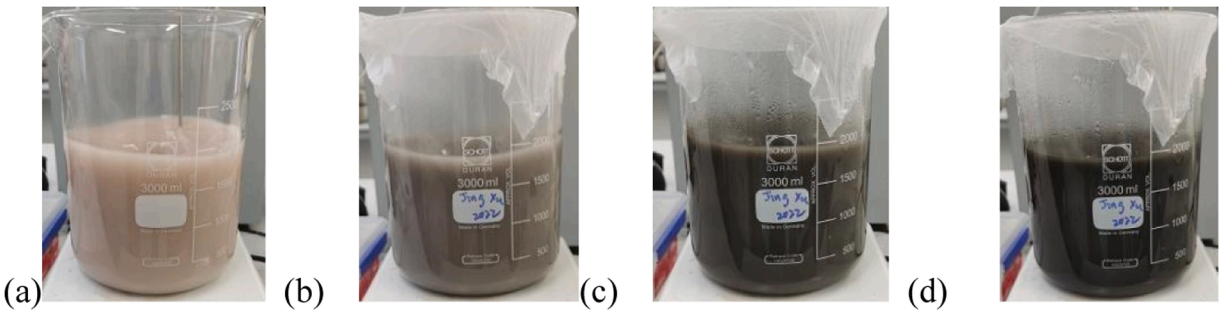

Fig. 1. Time-dependent self-polymerization of dopamine on mussel shell powders: (a) 0 min, (b) 10 min, (c) 1 h, (d) 24 h.

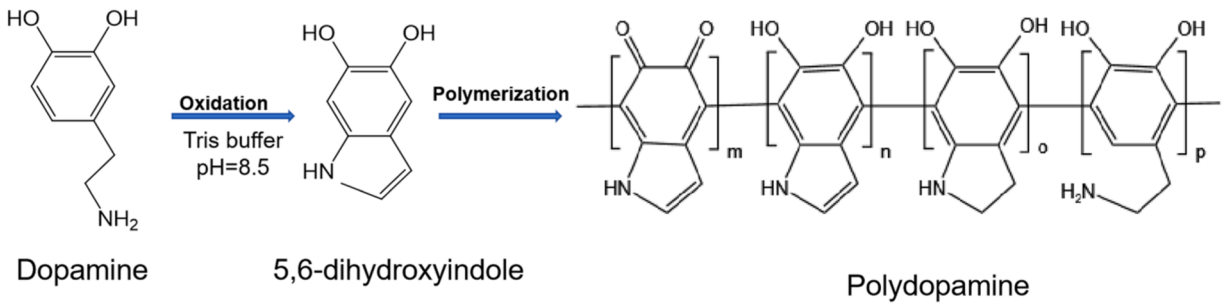

Fig. 2. The envisaged self-polymerization process of polydopamine from dopamine [35].

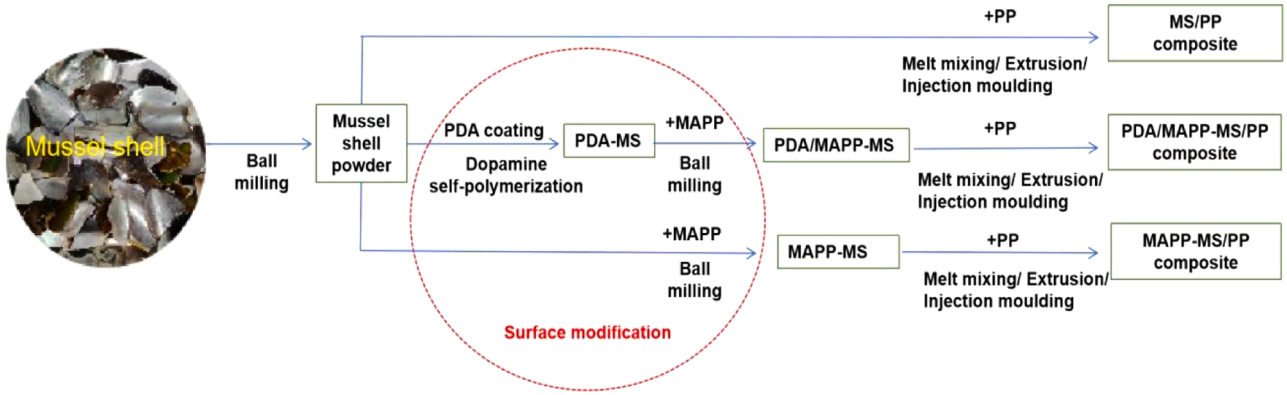

Fig. 3. A schematic illustrating the synthesis procedure of PP composites incorporated with different mussel shell fillers.

Table 1
Sample formulation and code names of materials studied.

Sample	PP (wt%)	MAPP (wt%)	MS (wt%)	PDA-MS (wt%)
PP	100	–	–	–
5%MS/PP	95	–	5	–
5%MAPP-MS/PP	92	3	5	–
5%PDA/MAPP-MS/PP	92	3	–	5
20%MS/PP	80	–	20	–
20%MAPP-MS/PP	77	3	20	–
20%PDA/MAPP-MS/PP	77	3	–	20

2.3.4. Particle size distribution

The size distribution profiles of commercial $CaCO_3$, mussel shell powder, PDA-MS powder, MAPP-MS powder, PDA/MAPP-MS powder were obtained through laser diffraction analysis using a Malvern Mastersizer 3000. Three repetitions were conducted for each sample, and the average data was obtained to determine the particle size distribution.

2.3.5. X-ray photoelectron spectroscopy (XPS)

XPS analysis was performed with a Thermo Fisher Scientific X-ray photoelectron spectrometer. The instrument operated at 200 W with an anode voltage of 12 kV, while maintaining a constant pressure of 2.0×10^{-7} mbar in the analysis chamber. Pass energies were set at 150 eV and 50 eV for survey and narrow scans, respectively. Peak fitting and background subtraction were performed using Thermo Scientific Avantage software (Version 5.948). The binding energies (BEs) were calibrated against adventitious carbon (C1s BE= 284.8 eV). Core peak analysis utilized a nonlinear Shirley-type background subtraction. Additionally, narrow scan spectra were analyzed using a weighted least-squares fitting approach, with peak positions and areas deconvoluted using a combination of 70% Gaussian and 30% Lorentzian line shapes.

2.3.6. Contact angle and surface energy

Contact angle measurements were conducted using a sessile drop method on compressed disk of untreated or treated mussel shell powder at room temperature (20±3 °C). A 10 μL test liquid was carefully delivered onto the surface of the test pellet with an auto-pipette. Images were captured within 20 s of application with a smartphone camera, then the contact angle was determined using the Image J contact angle plugin. Five measurements were taken at different spots on each sample and standard deviations were calculated accordingly. Distilled water and diiodomethane were used for measuring contact angles, and the surface energy of solid samples was calculated accordingly. The surface energy components of these liquids, required for the calculations, are provided in Table 2.

2.3.7. Scanning electron microscopy (SEM)

SEM images were obtained on fractured surfaces of PP composites filled with 5 wt% of the various fillers studied (viz., commercial $CaCO_3$, pristine mussel shell, MAPP-MS, and PDA/MAPP-MS) after tensile testing. The analysis was conducted with a Hitachi S-4700 Field Emission Scanning Electron Microscope at 5 kV.

2.3.8. Tensile and flexural tests

Tensile testing was conducted according to EN ISO 527 standards using an Instron® 5982 equipped with a 5 kN load cell, operated at a speed of 5 mm/min. Flexural testing was carried out in accordance with

Table 2
Polar and dispersive surface energy components of the test liquids [63].

	γ_l (mJ/m^2)	γ_l^p (mJ/m^2)	γ_l^d (mJ/m^2)
Water (W)	72.8	51.0	21.8
Di-iodomethane (DIM)	50.8	0.0	50.8

Note: γ_l is denoted as the surface energy of the test liquid; γ_l^p and γ_l^d are denoted as polar and dispersive surface energy components of the test liquid, respectively.

ASTM D790–17 [43]. Prior to testing, specimens were conditioned in a chamber maintained at 23 °C and 50% relative humidity for 48 h. A minimum of four composite samples were tested per condition to ensure robust statistical analysis, and results were reported as averages.

3. Results and discussion

3.1. FTIR and SS-NMR

Infrared spectroscopy is an effective tool for identifying the various phases of calcium carbonate due to the distinctive absorption bands that each phase displays in its spectrum. The carbonate ion exhibits four vibrational modes: two non-degenerate modes (symmetric stretching ν_1 at approximately 1085 cm^{-1} and out-of-plane bending ν_2 at approximately 860 cm^{-1}) and two doubly degenerate modes (asymmetric stretching ν_3 at approximately 1475 cm^{-1} and in-plane bending ν_4 at approximately 700 cm^{-1}) [44]. Among these, the ν_4 band is the most useful for determining calcium carbonate polymorphs, as it is sharp and distinct for crystalline phases such as calcite, aragonite, and vaterite. In mollusc shells, calcite and aragonite phases are evident, whereas vaterite is rarely encountered and typically confined to sites of shell regeneration. The infrared (IR) bands associated with aragonite and calcite are listed in Table 3 [22,44]. The two split peaks at ~700 cm^{-1} are characteristic of the aragonite structure, whereas calcite shows only one sharp unsplit peak at this position. Additionally, the symmetric stretching (ν_1) at 1085 cm^{-1} is more pronounced for aragonite, and the position of the out-of-plane bending ν_2 is also slightly different; the peak at 877 cm^{-1} is characteristic of calcite, while the peak at 857 cm^{-1} is characteristic of aragonite. Ding et al. investigated the FTIR spectra of *C. farreri* and identified different polymorphs at the interface and nacre layer based on the ratio of the peaks at 857 and 877 cm^{-1}. This observation suggests the coexistence of aragonite and calcite crystal forms in *C. farreri* [45]. Lee et al. identified the exclusive presence of aragonite in the nacre, whereas the polymorph in the folia layer of oyster shells was identified as calcite based on the in-plane bending ν_4 band, which split in the nacre sample but appeared as a single peak in the folia [46].

The FTIR spectra of the mussel shell, polydopamine modified mussel shell, and commercial $CaCO_3$ are shown in Fig. 4(a). Characteristic absorption peaks of calcium carbonate can be seen spanning 400 to 1700 cm^{-1}. In Fig. 4(a)-C, commercial $CaCO_3$ shows typical characteristic peaks for calcite, as ν_4 at 712 cm^{-1}, ν_2 at 875 cm^{-1}, and ν_3 at 1419 cm^{-1}, demonstrating the exclusive presence of the calcite polymorph in the commercial material. In contrast, the FTIR spectra of mussel shell (both pristine and polydopamine modified) display characteristic bands of both the calcite and aragonite phases. The in-plane bending (ν_4) splits into two peaks, 700 and 713 cm^{-1}, together with the symmetric stretching (ν_1) at 1085 cm^{-1}, indicating the presence of the aragonite structure [8,47]. Additionally, the out-of-plane bending band (ν_2) splits into two peaks, 859 and 875 cm^{-1}, representing aragonite and calcite structures, respectively. The intensity of the peak located at 859 cm^{-1} is relative stronger than that at 875 cm^{-1}, suggesting that aragonite is the predominant crystal form in mussel shells [45].

Table 3
Infrared band assignments for aragonite and calcite [22,43].

Crystal phases of $CaCO_3$	Assignment	Wavenumber (cm^{-1})
Aragonite	In-plane bending (ν_4)	713, 700
	Out of plane bending (ν_2)	859
	Asymmetric stretching (ν_3)	1475
	Symmetric stretching (ν_1)	1085
	Combination of $\nu_1 + \nu_3$	2521
	Combination of $\nu_1 + \nu_4$	1790
Calcite	In-plane bending (ν_4)	712
	Out of plane bending(ν_2)	875
	Asymmetric stretching mode (ν_3)	1419
	Symmetric stretching (ν_1)	–
	Combination of $\nu_1 + \nu_3$	2513
	Combination of $\nu_1 + \nu_4$	1800

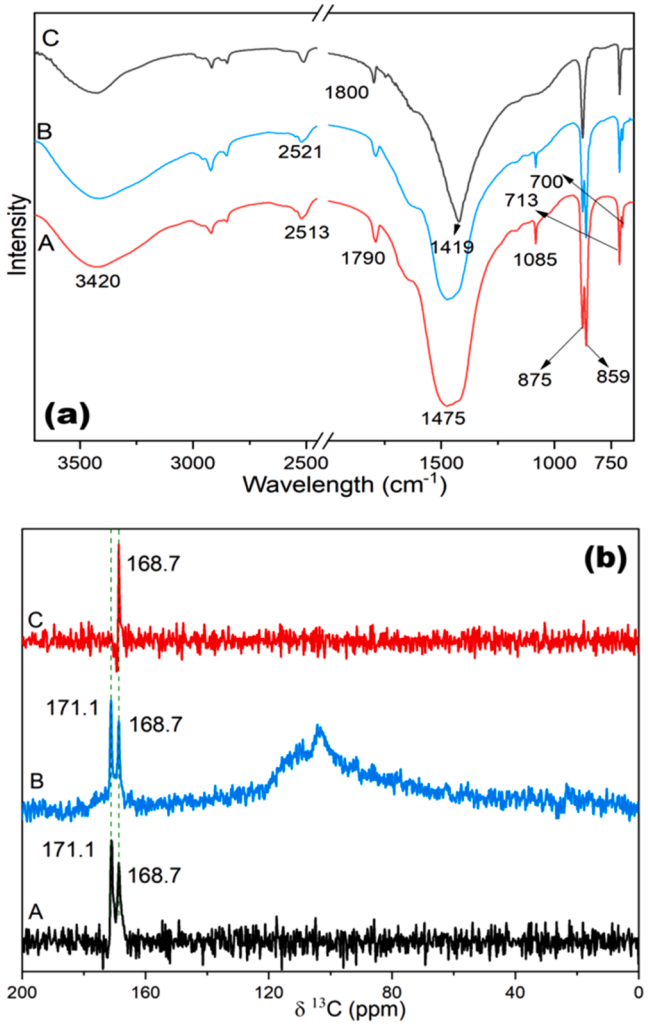

Fig. 4. FTIR(a) and ^{13}C MAS SS-NMR (direct polarization) (b) spectra of (A) mussel shell, (B)PDA-MS and (C) commercial $CaCO_3$.

The strongest absorption band (1600-1100 cm^{-1}) observed in mussel shell is broad and lacks sharpness, contrasting with the sharp band at 1419 cm^{-1} in commercial $CaCO_3$. This difference is likely due to overlapping peaks arising from the asymmetric stretching (ν_3) of aragonite (at 1475 cm^{-1}) and calcite (at 1419 cm^{-1}), along with the stretching vibration of C = C bonds, very likely originating from the organic matrix present in shells [45].The stretching vibration of C—O or C—N was identified at approximately 1630 cm^{-1}, while the stretching vibration of O—H or N—H was observed around 3415 cm^{-1}. These peaks correspond to the protein amide I (around 1650 cm^{-1}) and protein amide A (around 3415 cm^{-1}) peaks, indicating the presence of a protein matrix in mussel shells [45,48].

Yao et al. compared two fillers for polypropylene composites: mineral $CaCO_3$ and a bio-based filler derived from shell waste. The latter fillers were found to disperse more easily in the polymer matrix., likely due to the presence of matrix protein in the shell waste [32]. Similarly, in the present study, improved dispersion of mussel shell in polypropylene can be expected, as indicated by the FTIR spectra revealing the coexistence of organic and mineral phases in the mussel shell.

Solid-state NMR represents a well-established methodology for discerning the crystalline polymorphs inherent in calcium carbonate. The SS-NMR spectra of the mussel shell, PDA-MS, and commercial $CaCO_3$ are depicted in Fig. 4(b). Previous investigations into biogenic and geogenic $CaCO_3$ have consistently revealed that a chemical shift at

171.1 ppm signifies the carbonate typical of the aragonite crystalline form, while a shift at 168.7 ppm denotes the calcite form [24,49,50]. As shown in Fig. 4(b)-C, only one peak is evident at 168.7 ppm for commercial calcium carbonate, thereby confirming its exclusive polymorph identity as calcite. In contrast, the SS-NMR spectra of unmodified (Fig. 4 (b)-A) and polydopamine-coated mussel shells (Fig. 4(b)-B) show two discernible peaks within the 165- 175 ppm range: one at 171.1 ppm, characteristic of aragonite, and the other at 168.7 ppm, indicative of calcite. The coexistence of aragonite and calcite crystal forms in both unmodified and PDA-coated mussel shells was demonstrated by SS-NMR. A broad peak ranging from 60 to 120 ppm is observed in the SS-NMR spectrum of PDA-coated mussel shells. This peak can be attributed to contamination from C-F compounds in the rotor cap, which overlaps with the carbon signals originating from PDA.

The SS-NMR findings align well with those obtained through Fourier-transform infrared (FTIR) analysis.

3.2. XRD

The crystal structures and phase compositions of mussel shell, polydopamine-modified mussel shell (PDA-MS), and commercial calcium carbonate ($CaCO_3$) can be further elucidated by their XRD patterns, as shown in Fig. 5. The crystal phase of commercial $CaCO_3$ can be indexed to calcite (JCPDS PDF Card No. 47–1743). The characteristic planes of (012), (104), (110), (113), (202), (018), (116), (211), and (122) correspond to 2θ positions of 23.0°, 29.3°, 35.9°, 39.3°, 43.0°, 47.4°, 48.4°, 56.4°, and 57.3°, respectively, all of which are assigned to the calcite structure. Therefore, it can be concluded that the commercial $CaCO_3$ exclusively exhibits peaks attributed to the calcite phase. Both pristine mussel shell and PDA-MS revealed two main crystalline forms. In addition to the peaks corresponding to the calcite phase, peaks reflecting the aragonite phase were also detected at 2θ positions of 26.1°, 27.2°, 33.1°, 37.8°, and 38.4°, corresponding to the crystall planes (111), (021), (012), (200), (112), and (130), respectively (indexed to JCPDS PDF Card No. 41–1475). Notably, no peaks indicative of other non-$CaCO_3$ phases were detected in either the mussel shell or PDA-MS samples, suggesting a high level of raw material purity. Furthermore, the surface modification with polydopamine did not appear to affect the crystalline phases of the mussel shell.

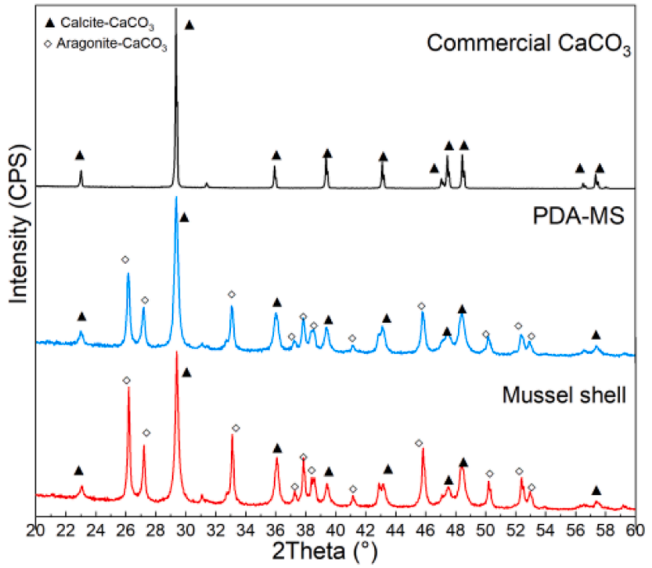

Fig. 5. XRD of commercial $CaCO_3$, mussel shell, PDA-MS.

3.3. Particle size distribution

Fig. 6 illustrates the particle size distribution (a) and cumulative curves (b) of commercial $CaCO_3$ alongside various mussel shells. Particle size distribution, adhesion at the particle-matrix interface, and particle loading levels significantly impact the mechanical properties of particulate-polymer composites [9,29,51]. Hence, it is imperative to investigate the size distribution of commercial $CaCO_3$ as well as untreated and surface-modified mussel shells.

As shown in Fig. 6, the commercial $CaCO_3$ exhibits a relatively narrow size distribution, ranging from 5 to 100 μm, with 100% of the grain population smaller than 100 μm. Similarly, 90 % of grains in the pristine mussel shell and PDA-MS samples were also smaller than 100 μm, although this proportion drops to 80 % of the total following MAPP or PDA/MAPP co-modification. The cumulative curve revealed that the majority of these fillers fall within the same size range ($10 < D_{50} < 50$ μm), which is considered to be relatively small. Larger particles, with a median size (D_{50}) of approximately 3 mm, have been observed to integrate efficiently into polymers [27]. Conversely, smaller particles with higher surface area tend to agglomerate due to increased particle-particle interactions [29]. This agglomeration can result in adverse dispersion and performance issues in the polymer composites.

The particle size distribution results suggest that all tested fillers have a tendency to agglomerate. Therefore, investigating the surface properties of these fillers is essential for understanding their agglomeration behaviour, particularly during processing with the polymer

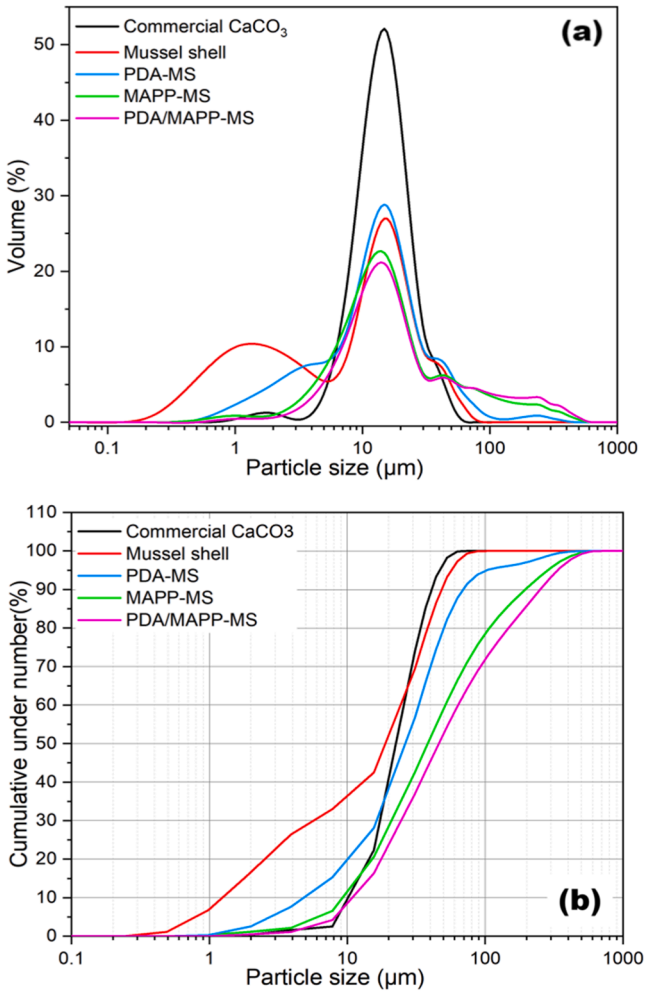

Fig. 6. The particle size distribution (a) and cumulative curves (b) of commercial $CaCO_3$ and different mussel shells.

matrix. Such insights will help determine the interfacial reactions of filler-matrix, which are crucial for assessing their influence on the mechanical performance of the PP composites.

3.4. XPS

XPS provides the surface elemental compositions, characteristics, chemical states, and distribution of functional groups in mussel shell, polydopamine (PDA), and PDA-modified surfaces (PDA-MS), as shown in Figs. 7 and 8. Elemental compositions are shown in Table 4.

The X-ray photoelectron survey spectrum (Fig. 7) of mussel shell and PDA-MS revealed the presence of the three elemental constituents of $CaCO_3$, namely Ca, C, and O. A weak signal attributed to N1s (atomic percentage of N= 1.56%) was also observed in the mussel shell, likely due to the presence of shell proteins.

According to the structural model of PDA as outlined in Fig. 2, XPS signals corresponding to C1s, N1s, and O1s were identified in the survey spectrum of polydopamine (Fig. 7, black line). The atomic percentage of N1s was reported to be 7.77%, originating from the amine groups of PDA. The N/C atomic ratio (0.11) of the polydopamine (PDA) synthesized in this research matches the reported value (N/C = 0.10) from a previous XPS investigation on PDA, suggesting a comparable structure for the obtained PDA [35].

In comparison to the N1s signal observed for the mussel shell alone, an enhanced signal for the N1s (atomic percentage of N= 4.32 %) was observed on the polydopamine-coated mussel shell (PDA-MS), This enhancement stems from the nitrogen-containing chemical groups introduced through the PDA coating. This observation provides evidence supporting the effective surface coating of polydopamine on the mussel shell. Furthermore, compared to the survey spectrum of PDA, the N/C ratio of PDA-MS decreased to 0.06, attributed to the incorporation of additional carbon atoms from carbonate and mussel protein.

To further elucidate the surface compositions of mussel shell, PDA, and PDA-MS, the narrow scan and curve fitting of the C 1 s, N 1 s, and O1s regions were acquired and presented in Fig. 8.

The high-resolution (narrow scan) spectrum of Ca 2p core levels in both mussel shell and PDA-MS samples reveals two peaks corresponding to the spin-orbit coupling peaks of Ca 2p (3/2) and Ca 2p (1/2), with a constant of approximately 3.5 eV, consistent with typical literature values [52].

For the binding energy values and their corresponding assessments of mussel shell, PDA, PDA-MS, the C1s region narrow scan is able to have three similar components fitted to it but with different intensities. Notably, the narrow scan profiles obtained for PDA and PDA-MS exhibit greater similarity to each other, whereas the profile for mussel shell alone appears more distinct. This indicates a comparable percentage of contribution from each functional group in these two samples. Specifically, discernible peaks corresponding to aliphatic carbon (or a hydrocarbon environment) were observed at a binding energy (BE) of 284.7 eV, while peaks attributable to C—O/C—N appeared at BE=286.4 eV, and those associated with C = O or carbonate groups were identified at BE=288.86 eV [53]. On comparison of pristine mussel shell and PDA-MS, the peaks at 286.4 and 288.86 eV were heightened for PDA-MS, indicating the presence of chemical groups containing C—O, C—N, and C = O which would have been introduced by the PDA coating. This result confirms the successful surface coating of polydopamine onto the mussel shell substrate.

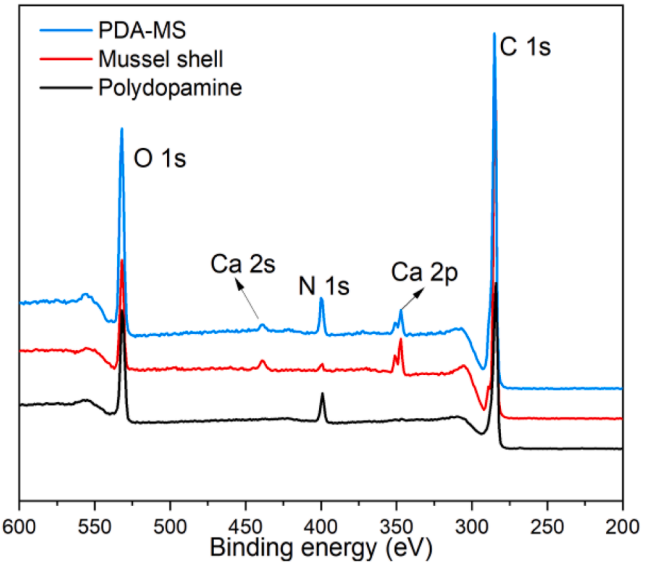

Fig. 7. XPS survey spectra of mussel shell, polydopamine, and polydopamine coated mussel shell (PDA-MS).

The O1s spectrum of the pristine mussel shell exhibits two main peaks: one attributed to CO_3^{2-} at a binding energy (BE) of 531.7 eV and another to O—H at 533.3 eV. Conversely, the O1s spectrum of polydopamine (PDA) reveals three principal peaks following deconvolution: C = O (BE=531.5 eV) originating from quinone and catechol, C—O (BE=532.7 eV), and O—H (BE=533.6 eV), respectively [54]. Upon PDA coating, the O1s spectrum of PDA-MS shows two predominant contributions align with those observed in the mussel shell [55].

The relatively weak N1s spectrum of the mussel shell can be deconvoluted into four components, including R = N-R (398.3 eV), C—NR_2 (399.4 eV), N—C = O (400.3 eV), and oxidized nitrogen groups such as O = C—N-C = O (401.00 eV). This complexity arises from the presence of the shell proteins [56], aligning with the findings from FTIR analysis. In accordance with the N1s spectrum of polydopamine, PDA-MS exhibits a broad and strong peak centred at 399.7 eV, indicative of C—NR_2 from rich amine compounds containing polydopamine, thereby further confirming the successful coating of polydopamine on the mussel shell [57].

3.5. Contact angle and surface energy

According to thermodynamic principles, surface energy (γ) and its constituent components represent crucial surface characteristics of solids, influencing their interactions with other materials [58-61]. For instance, the weak adhesive properties of polypropylene (PP) to binders, particularly those featuring polar surfaces, can be attributed to its non-polar nature characterized by a low surface energy (≈32 mJ/m^2) [62,63]. In polymer composites, these surface energy parameters govern filler dispersion and its adhesion to the polymer matrix.

To explore this aspect in our study, surface energies were calculated for both mussel shells and modified mussel shells using contact angle experiments. Given the absence of a precise algorithm, the Fowkes model, a commonly used semi-empirical method, was employed for this calculation [64].

$$\frac{\gamma_l(\cos\theta+1)}{2} = \left(\gamma_l^d\right)^{1/2}\left(\gamma_s^d\right)^{1/2} + \left(\gamma_l^p\right)^{1/2}\left(\gamma_s^p\right)^{1/2} \quad (1)$$

$$\gamma_s = \gamma_s^d + \gamma_s^p \quad (2)$$

Herby γ_l and γ_s is denoted as total surface energy of liquid and solid, respectively. θ is contact angle measured using a different test liquid. The superscripts d and p denote the dispersed and the polar part of the surface energy, respectively. When test liquid diiodomethane ($\gamma_l^p = 0$), is applied, the surface energy of solid(γ_s^d) can be calculated with Eq. (1). Subsequently, testing with a polar protic liquid, such as water, allows for the computation of the polar component of the solid surface energy γ_s^p, using γ_s^d and Eq. (1). In this context, the dispersive component denotes the interactions arising from London dispersion forces, while the polar component encompasses interactions induced by polar functional groups, such as hydroxyl, carboxyl, or amino moieties [64]. Eq. (2) expresses Fowkes' theory assumption that the total surface energy is the

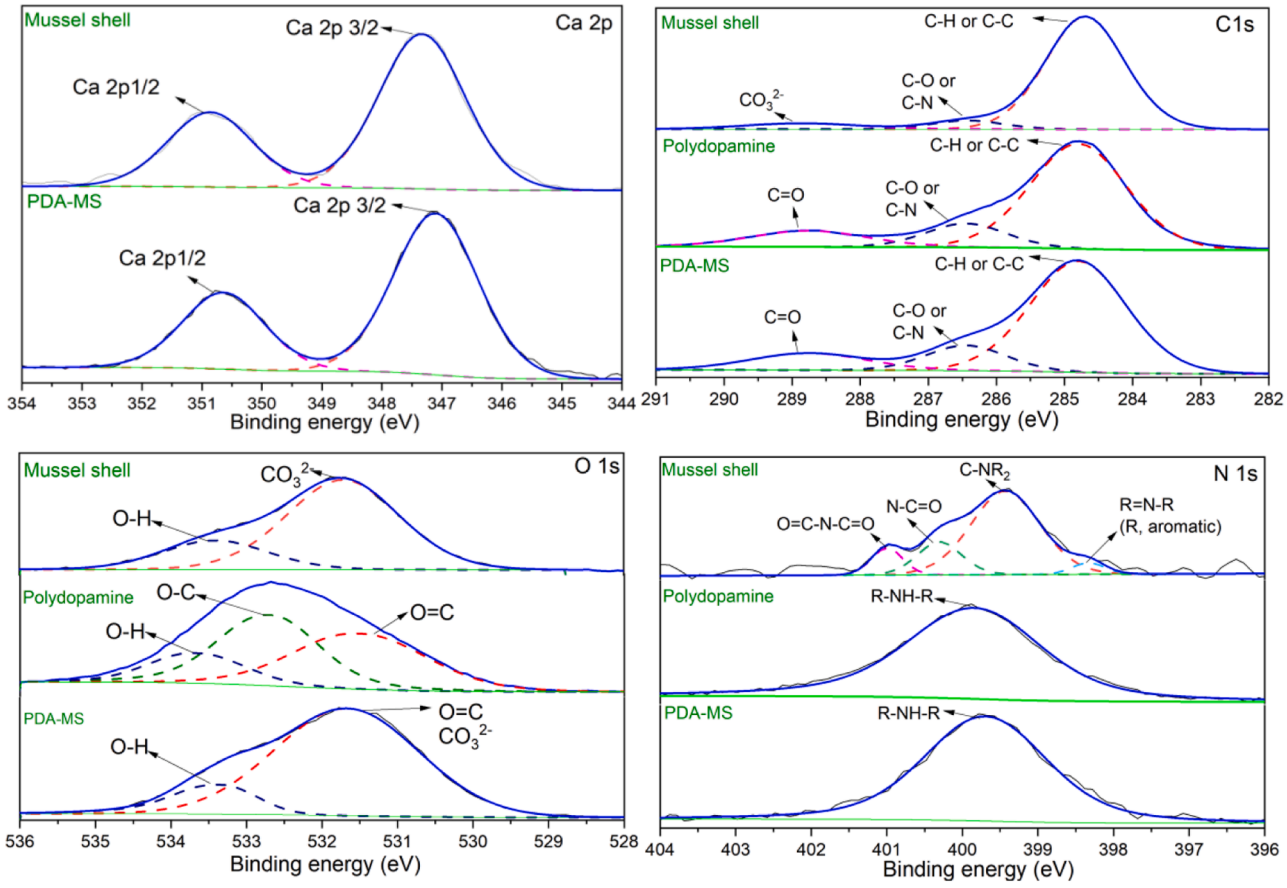

Fig. 8. High-resolution (narrow scan) XPS spectra of Ca 2p, C 1 s, O 1 s, and N 1 s regions of mussel shell, polydopamine, and PDA-MS.

Table 4
XPS surface elemental-analysis parameters of mussel shell, PDA, and PDA-MS.

Sample	Elemental contents					
	C(%)	N(%)	O(%)	Ca(%)	N/O	N/C
MS	83.53	1.56	12.69	2.21	0.12	0.02
PDA	71.31	7.77	20.93	–	0.37	0.11
PDA-MS	69.1	4.32	23.54	3.04	0.18	0.06

sum of dispersive and polar surface energies. This analysis facilitates understanding the surface properties of mussel shell fillers before and after various surface modifications, thereby predicting filler dispersion and interfacial adhesion to the matrix.. The results of these analyses are summarized in Table 5.

Following the PDA coating on mussel shell surfaces, contact angles (CAs) obtained with two test liquids show distinct trends compared to those on untreated mussel shells. Specifically, after PDA coating, the contact angle from the water test (CA_W) decreases, while the contact angle from the diiodomethane test (CA_{DIM}) increases slightly. These results are consistent with previous findings suggesting that the observed changes stem from the introduction of hydrophilic functional groups-such as hydroxyl, amine, and imine groups onto the mussel shell surface through the PDA coating, which enhances the surface hydrophilicity [60]. Accordingly, the polar surface energy of untreated mussel shell is 24.6 mJ/m^2, while that of PDA coated mussel slightly increased to 25.9 mJ/m^2. [45]

The surface energy calculation reveals that the PDA coating does not enhance the mussel shell's hydrophobicity. The main goal of PDA coating is to introduce functional groups like amines and hydroxyls onto the shell surface. These functional groups, coupled with aromatic

Table 5
Contact angles (average (standard deviation)), surface energies and the potential energy differences.

Samples	Contact angle (°)		Surface energy (mJ/m^2)			cos θ	ΔWa (mJ/m^2)
	CA_W	CA_{DIM}	γ_s^p	γ_s^d	γ_s		
MS	29.3 (2.2)	14.3 (2.6)	24.6	49.2	73.8	0.13	46.44
PDA-MS	26.4 (3.5)	15.4 (2.4)	25.9	49.0	74.9	0.11	48.80
MAPP-MS	87.5 (28)	49.1 (3.6)	2.1	34.8	36.9	0.86	2.63
PDA/MAPP-MS	103.6 (5.1)	48.9 (2.4)	0.001	34.9	34.9	0.94	0.23
PP[2]	108		0.1	32.8	32.9		
PP[1]	98(2.3)	57(0.8)	0.5	31.6	32.1		

Note: γ_s is denoted as total solid surface energy; γ_s^p and γ_s^d are denoted as polar and dispersive surface energy components of solid, respectively; ΔWa is denoted as the potential energy difference.

structures, enable PDA coating to interact effectively with additional surface modification reagents, such as MAPP. This bridging occurs through mechanisms including hydrogen bonding, covalent bonding, π-π conjugation, and chemical bonds, such as ester bonds.

In contrast to untreated MS or PDA-MS, the dispersive and polar energies of the surface modified MAPP-MS sample decreased significantly, and further reduction is moreover realized with the PDA/MAPP co-modified mussel shell fillers, bringing their surface energies closer to the values reported for PP alone [62,63]. In particular, the polarity component of surface energy decreased by over 90 % for both MAPP-MS

and PDA/MAPP-MS. This substantial decrease effectively represents an increased hydrophobicity achieved via MAPP modification alone or when the MAPP is combined with PDA-coated mussel shell fillers.

Aggregated fillers typically result in defects within polymer composites, hindering filler-matrix interaction. Consequently, the mechanical properties of the composite materials are compromised. To assess the tendency of fillers to aggregate during the initial processing stages of compounding polymer composites, the Owens-Wendt model was applied to calculate cosθ (equivalent equilibrium contact angle) as presented in Eq. (3) and 4 [58]. Hereby, γ_{PP} is denoted as the total solid surface energy of PP while γ_{Filler} is denoted as the total solid surface energy of filler, respectively.

$$\cos\theta = -1 + 2\frac{\sqrt{\gamma_{PP}{}^{d}\gamma_{Filler}{}^{d}}}{\gamma_{Filler}} + 2\frac{\sqrt{\gamma_{PP}{}^{p}\gamma_{Filler}{}^{p}}}{\gamma_{Filler}} \tag{3}$$

$$\cos\theta = \begin{cases} -1 + 2\dfrac{W_{FP}}{W_{FF}} & \dfrac{W_{FP}}{W_{FF}} < 1 \\ 1 & \dfrac{W_{FP}}{W_{FF}} > 1 \end{cases} \tag{4}$$

The work of adhesion (W) is the energy required to separate the two adjacent phases. W_{FF} represents the work of adhesion of two filler particles, while W_{FP} is denoted as the work of adhesion between filler-polymer.

According to Eq. (4), Natarajan *et al.* proposed that when cosθ< 1, fillers tend to aggregate to minimize interfacial energy, as the relative attraction between fillers (W_{FF}) is more significant than between fillers and the polymer matrix (W_{FP}). This indicates an initial lack of dispersion state for these fillers [65]. As shown in Table 5, when considering PP as the matrix, the cosθ values for four different fillers—untreated mussel shell fillers, PDA-MS, MAPP-MS, and PDA/MAPP-MS—are all below 1. This indicates a propensity for these fillers to aggregate upon incorporation into the PP matrix. However, the cosθ value of MAPP-MS ($cos\theta$ = 0.86) significantly exceeds that of untreated mussel shell fillers ($cos\theta$ = 0.13), indicating an improvement in initial dispersibility of mussel shells through MAPP modification. Furthermore, the highest cosθ value ($cos\theta$ = 0.94) obtained from PDA/MAPP-MS indicates that the PDA coating before MAPP modification can act to further improve the dispersibility of mussel shells. The observed effect is credited to the bridging impact of the PDA coating between MAPP and the mussel shell.

$$\Delta Wa = W_{FF} + W_{PP} - 2W_{FP} \tag{5}$$

$$\Delta Wa = 2\left(\sqrt{\gamma_{Filler}{}^{d}} - \sqrt{\gamma_{PP}{}^{p}}\right)^{2} + 2\left(\sqrt{\gamma_{Filler}{}^{p}} - \sqrt{\gamma_{PP}{}^{p}}\right)^{2} \tag{6}$$

According to thermodynamic theory, the initial dispersed fillers tend to re-agglomerate during subsequent processing for compounding polymer composite. To evaluate the driving force behind filler re-aggregation within polymer matrix, the difference of potential energy (ΔWa) between the filler-filler adhesion energy (W_{FF}) and the polymer-polymer adhesion energy (W_{PP}), formed by the filler-polymer adhesion energy (W_{FP}), is crucial, as illustrated in Eq. (5) and 6 [66]. Essentially, the larger the ΔWa, the greater the potential for filler re-agglomeration when processed with polymer. Table 5 presents the ΔWa values of different mussel shell fillers in PP matrix.

In polypropylene (PP) composites, the ΔWa value for MAPP-MS fillers was calculated to be 2.63 mJ/m^2, representing a clear decrease compared to that of pristine mussel shell fillers (ΔWa =46.44 mJ/m^2) or PDA-MS fillers (ΔWa = 48.80 mJ/m^2). The lowest ΔWa value (0.23 mJ/m^2) was obtained for the PDA/MAPP-MS filler in the PP system, indicating a significantly reduced tendency for re-agglomeration of these fillers. This substantial reduction suggests a low propensity for re-agglomeration of MAPP-MS and PDA/MAPP-MS fillers within polypropylene. Consequently, improved compatibility can be anticipated between the polypropylene matrix and MAPP-modified mussel shell fillers, with further enhancement expected when mussel shells undergo MAPP modification after polydopamine coating.

3.6. SEM

Contact angle experiments reveal that after MAPP or PDA/MAPP co-modification, the surface of mussel shells becomes more hydrophobic, and their surface energies approach that of PP, suggesting better compatibility in accordance with the principle of "like dissolves like" [48].

SEM analysis provides insights into both the particle dispersion within the matrix and the potential adhesion between the two phases. The influence of surface modification on mussel shell fillers is directly observable from SEM analysis conducted on the fracture surfaces of the PP composites with different fillers. Fig. 9(a) and (b) depict SEM images of fracture surfaces of PP composites incorporating 5 wt% commercial $CaCO_3$ and 5 wt% unmodified mussel shells, respectively. Clear voids are observed between the fillers and the polymer, indicating extensive debonding of these fillers from the PP matrix due to a lack of total compatibility/adhesiveness. The absence of surface modification renders these fillers highly hydrophilic, resulting in poor adhesion with the hydrophobic PP matrix, as discussed in the previous section (3.5).

The efficacy of surface modification with MAPP or PDA/MAPP co-modification is clearly demonstrated in Fig. 9(c) and (d), where a notable enhancement in filler/matrix wettability supporting the potential for increased adhesion is observed, indicated by the absence of holes and debonding of the filler. Moreover, polymer fragments are observed adhered to the surface of the fillers, manifesting as pull-out pieces on the aggregated filler surface.

MAPP functions as a highly effective polymer composite compatibilizer, enhancing the interfacial adhesion between filler and matrix. The grafted maleic anhydride on the polypropylene chain facilitates the formation of strong interfacial adhesion by creating covalent ester bonds with the hydroxyl groups present on the fillers. Furthermore, during the melt processing stage, the polypropylene backbone of MAPP forms entanglements with the PP matrix, further improving compatibility. This mechanism has been documented in previous literature [26,67,68]. Although the effectiveness of MAPP as a polymer compatibilizer is well known, direct evidence of esterification between MAPP and fillers in polymers remains challenging to detect, even with cellulosic fillers containing abundant hydroxyl groups. The challenge arises because MAPPs typically contain only a few percent of acid functional groups. Additionally, as a compatibilizer, the amount of MAPP typically ranges from 3–5 wt%, further diluting the acid functional groups to less than 1% [69].

In this study, both pristine and polydopamine (PDA) coated mussel shells underwent MAPP modification through dry ball-milling. Subsequently, these modified fillers were incorporated into a polypropylene (PP) matrix through melt mixing, followed by extrusion and injection molding processes. Dry ball-milling, utilized for MAPP modification in this study, is a solid-state mechano-chemical treatment known for its ability to generate local high-pressure spots and facilitate closer contact between reacting species, potentially leading to novel chemical reactions. Previous reports have indicated the functionalization of multi-walled carbon nanotube fillers with MAPP to enhance its compatibility with PP [70]. Another study revealed that ball milling cellulose with MAPP has been shown to facilitate the release of -OH groups in crystalline cellulose, thereby inducing efficient esterification between cellulose hydroxyl groups and maleic anhydride groups in MAPP [71].

In the case of MAPP-MS, given that $CaCO_3$ is the primary chemical constituent of mussel shells, it is not surprising that functional groups such as -OH are absent. Consequently, the possibility of esterification between MAPP and mussel shells presents significant challenges. It is more probable that the process of coating MAPP onto the shells involves physical dispersion and surface coverage during the assisted-intensive ball milling process. The improved interfacial bonding between MAPP-

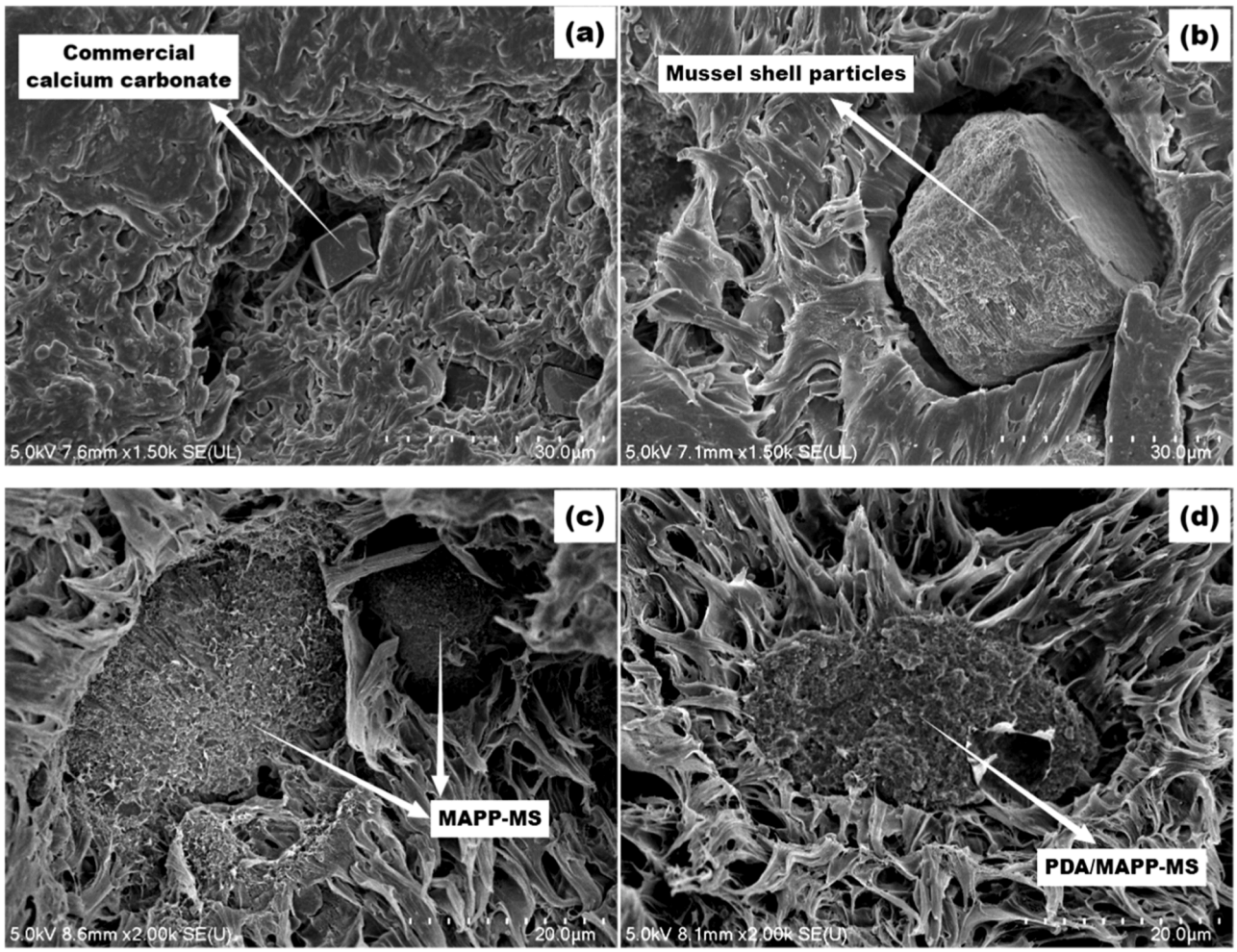

Fig. 9. SEM images of PP composites incorporated with (a) 5 % commercial $CaCO_3$ (b) 5 % pristine mussel shell (c) 5 % MAPP-MS (d) 5 % PDA/MAPP-MS.

MS and PP observed from SEM images is more likely to be attributed to the entanglement of PP and the PP backbone of MAPP during the subsequent melt mixing and extrusion process at high temperature (161–185 °C), as the mobility of polymer chains can be achieved above its melting temperature (melt point of PP is 140 °C in this study).

In PDA/MAPP-MS, the mussel shell surface is initially coated with polydopamine through self-polymerization, introducing functional groups like amines and catechols from PDA. During the ball-milling process, these functional groups on the surface of mussel shell can be effectively activated by localized high-pressure spots and close contact with maleic anhydride groups in MAPP, then these functional groups may react with maleic anhydride groups from MAPP through ring-opening reactions, leading to the formation of strong chemical bonding between the mussel shell and MAPP interfaces. Furthermore,

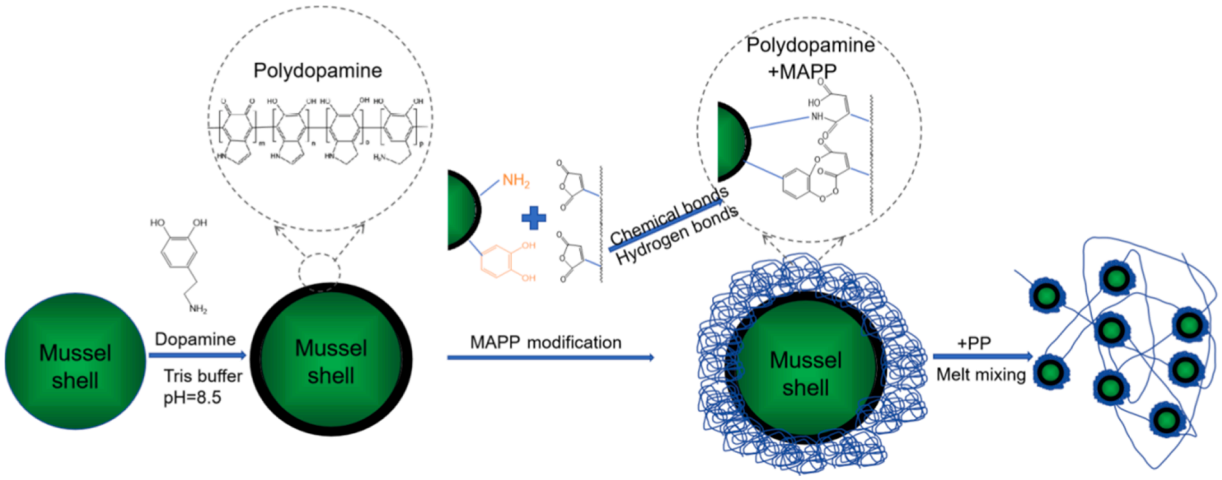

Fig. 10. Surface modification of mussel shell through PDA coating and MAPP modification.

during high-temperature melt mixing and extrusion (160–185 °C) procedures for compounding PP composites, the maleic anhydride groups readily undergo ring-opening to convert into dicarboxylic acid groups. This transformation potentially allows for hydrogen bonding with the amine groups present between the PDA-coated mussel shell and the matrix, thereby enhancing the interfacial adhesion of the composites. A schematic illustrating how the mussel shell becomes functionalised through PDA coating and MAPP modification is presented in Fig. 10.

3.7. Mechanical properties

As discussed in the previous sections, the surface properties of fillers in polypropylene composites can be effectively tailored through either MAPP modification or PDA/MAPP co-modification, leading to improvements such as increased hydrophobicity and reduced tendencies for filler agglomeration and re-agglomeration during processing. In order to probing the effect of mussel shell filler surface modification on the macroscopic properties of PP composites, tensile and flexural behaviour were investigated on the neat PP and PP composites incorporated with unmodified mussel shell fillers, MAPP modified mussel shell, and PDA/MAPP-modified mussel shell fillers were examined, respectively. Fig. 11(a) presents the representative stress-strain curves for these samples, while Fig. 11(b) compares their tensile strength and Young's modulus. Flexural strength and moduli are shown in Fig. 11(c), with all average values and corresponding errors provided in Table 6.

A filler loading level of 20 wt% was selected in this study to probe the influence of different surface modification techniques. More systematic studies on the mechanical properties of unmodified and surface-modified mussel shells at different loading levels will be the subject of a future publication. The stress-strain curves clearly show that incorporating these three different mussel shell fillers reduces the ductility of neat PP, as evidenced by a significant drop in elongation at break. This reduction is primarily due to the rigid nature of the particles, which do not deform under external stress but instead act as stress concentrators during deformation [11,72].

The inclusion of 20 wt% unmodified mussel shell fillers or MAPP-MS fillers led to a decrease in tensile strength compared to pure PP. Specifically, compared to the average tensile strength of pure PP (23.81 MPa), the tensile strength decreased by 11.1% and 7.8% for PP composites incorporating 20 wt% unmodified mussel shell fillers and MAPP-MS fillers, respectively.

Due to their hydrophilic nature and high tendency for agglomerate, the incorporation of unmodified mussel shell fillers into the PP matrix results in defects in the composite, such as voids and debonding, as observed around mussel shell fillers in SEM images. Moreover, the weak interface adhesion leads to less effective stress transfer between filler and matrix, resulting in poor tensile strength performance.

Despite the enhanced hydrophobicity resulting from MAPP modification, the incorporation of 20 wt% MAPP-modified mussel shell fillers into the PP still leads to lower tensile strength. Conversely, a 2.9% increase in tensile strength compared to neat PP is observed for 20% PDA/MAPP-MS/PP. As indicated by the potential energy difference (ΔWa) discussed in Section 3.5, the re-agglomeration tendency of MAPP-MS fillers in the PP matrix is approximately ten times higher than that of PDA/MAPP co-modified mussel shell fillers. Previous studies have proposed that the decrease in tensile strength can also be the consequence of filler agglomeration during initial processing and re-agglomeration during subsequent processing steps [18,47,48,73]. Tensile strength is particularly sensitive to filler dispersion and interfacial strength. Additionally, the overall strength of polymer composites is heavily influenced by the effectiveness of stress transfer between the fillers and the matrix [9,11]. Sufficient adhesion between fillers and the matrix facilitates efficient transfer of applied stress from the matrix to the particles, consequently the strength is enhanced [51]. Therefore, the improved tensile strength of 20% PDA/MAPP-MS/PP might be attributed to the fact that PDA/MAPP co-modification not only improves the hydrophobicity of mussel shell fillers, but also enables better filler dispersion, enhanced filler-matrix compatibility, and improved interfacial adhesion, supporting the mechanism proposed and illustrated in Fig. 10.

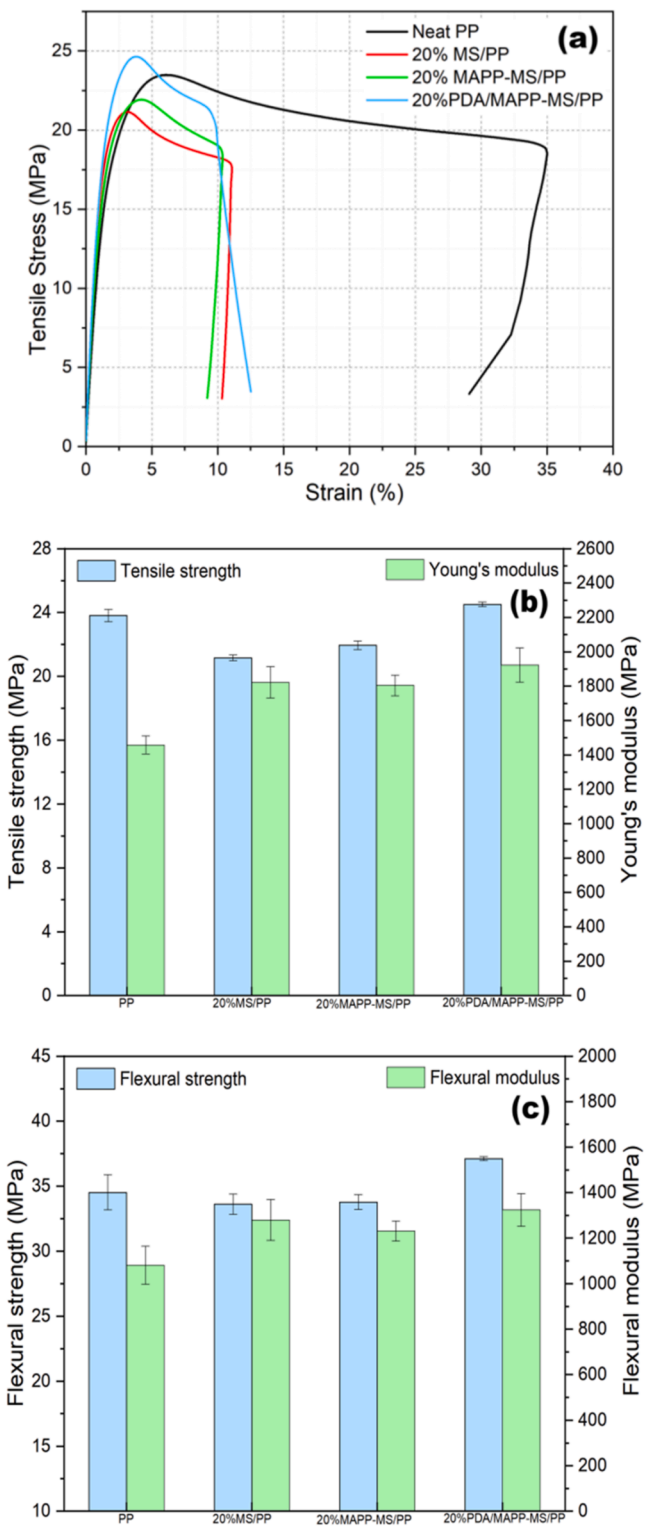

Fig. 11. Mechanical behaviour of PP and PP composites, (a) representative stress- strain curves, and (b) tensile strength and Young's modulus values, (c) flexural strength and modulus.

Regarding Young's modulus, PP composites containing 20% untreated or surface-modified mussel shell fillers exhibit higher modulus

Table 6
Mechanical properties of PP and PP composites.

Samples	Tensile strength (MPa)	Young's modulus (MPa)	Elongation at break (%)	Flexural strength (MPa)	Flexural Modulus (MPa)
PP	23.81 ±0.38	1458.22 ±53.03	29.71±6.85	34.52 ±1.35	1081.22 ±83.17
20%MS/PP	21.16 ±0.17	1822.22 ±91.24	12.85±4.35	33.61 ±0.78	1280.12 ±90.08
20%MAPP-MS/PP	21.95 ±0.27	1804.83 ±59.63	10.19±1.84	33.78 ±0.57	1231.29 ±44.25
20%PDA/MAPP-MS/PP	24.51 ±0.14	1923.39 ±98.93	8.42±1.83	37.12 ±0.16	1324.03 ±71.76

values compared to neat PP. This increase in stiffness is attributed to the incorporation of rigid inorganic particles, which generally possess higher stiffness than polymer matrices [72].

Similarly to tensile strength and modulus, PP composites containing 20% mussel shell or MAPP-modified mussel shell fillers exhibited a slight reduction in flexural strength compared to neat PP (34.52 MPa). However, 20% PDA/MAPP-MS/PP showed a 7.5% increase in flexural strength (37.12 MPa). These results further support that PDA/MAPP co-modification on mussel shell fillers lead to better filler dispersion within the matrix and enhanced filler-polymer interfacial adhesion. Additionally, all PP composites filled with 20% untreated, MAPP-, or PDA/MAPP-modified mussel shell fillers displayed higher flexural modulus values, indicating increased brittleness and stiffness due to the addition of rigid mussel shell fillers. These findings are in agreement with previous research. Yao *et al.* reported comparable improvements in the flexural properties of PP composites through the incorporation of furfural-modified clam shell fillers [32].

4. Conclusion

In this study, the crystal polymorphs and surface characteristics of mussel shell-derived calcium carbonate were investigated using various analytical techniques. With its predominant crystal phases of aragonite and calcite, along with an organic matrix, mussel shell was shown to be an attractive candidate for biogenic filler materials in polymer composites.

Inspired by the remarkable adhesive properties of mussels, polydopamine was explored as a facile method for surface functionalization of mussel shell. Surface energy calculations using the Fowkes model showed that PDA-coated mussel shell fillers retained the same level of hydrophilicity as unmodified fillers. However, the introduction of functional groups via PDA, confirmed by XPS, facilitated successful surface modification with MAPP through chemical and hydrogen bonding. It can be seen from the surface energy values that MAPP-modified mussel shell fillers exhibited improved hydrophobicity, while the tendencies of filler agglomeration and re-agglomeration were significantly reduced by the additional PDA/MAPP co-modification, as revealed using the Owens-Wendt model. Moreover, SEM images of the fracture surfaces of PP composites provided direct evidence of the interfacial adhesion between MAPP-MS or PDA/MAPP-MS filler and the PP matrix, while extensive debonding was contrastingly observed for the unmodified mussel shell and commercial calcium carbonate from the PP matrix due to a lack of adequate compatibility or adhesion.

Possible mechanisms for enhancing filler-matrix interaction were proposed. The interfacial adhesion between MAPP-MS and PP can be mainly attributed to entanglement between PP matrix and the backbone of MAPP on the surface of mussel shell during the melt processing. In the case of PDA/MAPP co-modification, the bridging effect of polydopamine through chemical bonds and hydrogen bonds resulted in better adhesion between mussel shell particles and MAPP, which in turn strengthened the interfacial adhesion for PDA/MAPP-MS fillers with PP. At a 20 wt% loading level, the tensile and flexural strength of PP composite with PDA/MAPP-MS fillers increased by 2.9% and 7.5%, respectively while unmodified mussel shell and MAPP-MS fillers resulted in deteriorated performance. Improvement of bulk performance further supports the notion that the dispersion, compatibility, and interfacial adhesion of filler-matrix can be enhanced with PDA/MAPP co-modification on mussel shell fillers.

This research demonstrates that mussel shells can serve as a biogenic source of $CaCO_3$, and their application as fillers in polymer composites repurposes shell waste, reducing production costs and enhancing the sustainability of fossil fuel-derived polymers. Thermodynamic analyses based on contact angle measurements provide guidance for optimizing filler surface properties through modification. This resulted in enhanced macroscopic properties of the polymer composites. These findings lay the foundation for future applications of mussel shell bio-fillers in alternative polymer composites.

CRediT authorship contribution statement

Jing Xu: Writing – review & editing, Writing – original draft, Methodology, Investigation, Formal analysis, Conceptualization. **Michael R. Mucalo:** Writing – review & editing, Supervision, Resources, Methodology, Formal analysis. **Kim L. Pickering:** Writing – review & editing, Supervision, Funding acquisition.

Declaration of competing interest

The authors declare that they have no known competing financial interests or personal relationships that could have appeared to influence the work reported in this paper.

Data availability

Data will be made available on request.

Acknowledgments

This research was supported by New Zealand MBIE Endeavour Fund-Amiomio Aotearoa research programme (UOWX2004). Jing also acknowledges the financial support provided by The University of Waikato through a Doctoral Scholarship and a Research & Enterprise Award (108023). JX also extends sincere gratitude to Professor Hun Xue from Fujian Normal University, China for her invaluable support with XPS characterization, and to Helen Turner from The University of Waikato for her insightful contributions to SEM characterization.

References

[1] S. Owuamanam, D. Cree, Progress of bio-calcium carbonate waste eggshell and seashell fillers in polymer composites: a review, J. Compos. Sci. 4 (2) (2020), https://doi.org/10.3390/jcs4020070.
[2] FAO, Fishery and Aquaculture Statistics – Yearbook 2021, FAO, Rome, 2024, https://doi.org/10.4060/cc9523en.
[3] A.S. Naik, M. Hayes, Bioprocessing of mussel by-products for value added ingredients, Trend. Food Sci. Technol. 92 (2019) 111–121, https://doi.org/10.1016/j.tifs.2019.08.013.
[4] T. H Silva, J. Mesquita-Guimarães, B. Henriques, F.S. Silva, M.C. Fredel, The potential use of oyster shell waste in new value-added by-product, Resources 8 (1) (2019) 13, https://doi.org/10.3390/resources8010013.
[5] J. Cangiotti, M. Scatto, E. Araya-Hermosilla, C. Micheletti, D. Crivellari, A. Balloni, et al., Valorization of seashell waste in polypropylene composites: an accessible solution to overcome marine landfilling, Eur. Polym. J. 162 (2022) 110877, https://doi.org/10.1016/j.eurpolymj.2021.110877.
[6] Ministry for the Environment. (2021). Waste disposal levy expansion. https://environment.govt.nz/what-government-is-doing/areas-of-work/waste/waste-disposal-levy/expansion/.
[7] C. Martínez-García, B. González-Fonteboa, D. Carro-López, F. Martínez-Abella, 8 - Recycled mollusc shells, in: J de Brito, F Agrela (Eds.), New Trends in Eco-efficient and Recycled Concrete, Woodhead Publishing, 2019, pp. 191–205, https://doi.org/10.1016/B978-0-08-102480-5.00008-7.

[8] P.M.A. Melo, O.B. Macêdo, G.P. Barbosa, M.M. Ueki, L.B. Silva, High-density polyethylene/mollusk shell-waste composites: effects of particle size and coupling agent on morphology, mechanical and thermal properties, J. Mater. Res. Technol. 8 (2) (2019) 1915–1925, https://doi.org/10.1016/j.jmrt.2019.01.008.

[9] S. Nwanonenyi, M. Obidiegwu, G. Onuegbu, Effects of particle sizes, filler contents and compatibilization on the properties of linear low density polyethylene filled periwinkle shell powder, Int. J. Eng. Sci. 2 (2) (2013) 1–8, https://doi.org/10.1016/j.biomaterials.2003.07.005.

[10] Z. Yao, M. Xia, L. Ge, T. Chen, H. Li, Y. Ye, et al., Mechanical and thermal properties of polypropylene (PP) composites filled with $CaCO_3$ and shell waste derived bio-fillers, Fiber. Polym. 15 (6) (2014) 1278–1287, https://doi.org/10.1007/s12221-014-1278-5.

[11] C. Kochan, F. Selli, U.H. Erdogan, Using mussel shell wastes as an additive for the production of thermally improved polypropylene composite monofilaments, J. Text. Eng. 112 (5) (2020) 683–690, https://doi.org/10.1080/00405000.2020.1776056.

[12] Z. Lin, Z. Guan, C. Chen, L. Cao, Y. Wang, S. Gao, et al., Preparation, structures and properties of shell/polypropylene biocomposites, Thermochim. Acta. 551 (10) (2013) 149–154, https://doi.org/10.1016/j.tca.2012.10.009.

[13] M.S. Xia, Z.T. Yao, L.Q. Ge, T. Chen, H.Y. Li, A potential bio-filler: the substitution effect of furfural modified clam shell for carbonate calcium in polypropylene, J. Compo. Mater. 49 (7) (2015) 807–816, https://doi.org/10.1177/00219983145259.

[14] V. Gigante, P. Cinelli, M.C. Righetti, M. Sandroni, L. Tognotti, M. Seggiani, et al., Evaluation of Mussel Shells Powder as Reinforcement for PLA-Based Biocomposites, Int. J. Mol. Sci. 21 (15) (2020), https://doi.org/10.3390/ijms21155364.

[15] T. Cecchi, A. Giuliani, F. Iacopini, C. Santulli, F. Sarasini, J. Tirillò, Unprecedented high percentage of food waste powder filler in poly lactic acid green composites: synthesis, characterization, and volatile profile, Environ. Sci. Pollut. Res. 26 (7) (2019) 7263–7271, https://doi.org/10.1007/s11356-019-04187-1.

[16] M.O. Lap, Y. Kanbur, Ü. Tayfun, The use of mussel shell as a bio-additive for poly (lactic acid) based green composites, Chem. Chem. Technol. 15 (4) (2021) 621–626, https://doi.org/10.23939/chcht15.04.621.

[17] S. Şişmanoğlu, Y. Kanbur, C.-M. Popescu, D. Kindzera, Ü. Tayfun, Beneficial use of mussel shell as a bioadditive for TPU green composites by the valorization of an aqueous waste, Waste Dispos. Sustain. Energy 6 (1) (2024) 123–137, https://doi.org/10.1007/s42768-023-00165-z.

[18] M.R.R. Hamester, P.S. Balzer, D. Becker, Characterization of calcium carbonate obtained from oyster and mussel shells and incorporation in polypropylene, Mater. Res. 15 (2) (2012) 204–208, https://doi.org/10.1590/s1516-14392012005000014.

[19] R. Karthick, P. Sirisha, M.R. Sankar, Mechanical and tribological properties of PMMA-sea shell based biocomposite for dental application, Proced. Mater. Sci. 6 (2014) 1989–2000, https://doi.org/10.1016/j.mspro.2014.07.234.

[20] B. Peceño, B. Alonso-Fariñas, C. Arenas, C. Leiva, Influence of particle size of mussel shells in physical, mechanical and insulating properties of fireproof materials Procedia Environmental Science, Eng. Manag. (2021).

[21] M.H. Chong, B.C. Chun, Y.-C. Chung, B.G. Cho, Fire-retardant plastic material from oyster-shell powder and recycled polyethylene, J. Appl. Polym. Sci. 99 (4) (2006) 1583–1589, https://doi.org/10.1002/app.22484.

[22] R. Ševčík, P. Šašek, A. Viani, Physical and nanomechanical properties of the synthetic anhydrous crystalline $CaCO_3$ polymorphs: vaterite, aragonite and calcite, J. Mater. Sci. 53 (6) (2018) 4022–4033, https://doi.org/10.1007/s10853-017-1884-x.

[23] P.N. Gavryushkin, A.B. Belonoshko, N. Sagatov, D. Sagatova, E. Zhitova, M. G. Krzhizhanovskaya, et al., Metastable structures of $CaCO_3$ and their role in transformation of calcite to aragonite and postaragonite, Cryst. Grow. Des. 21 (1) (2021) 65–74, https://doi.org/10.1021/acs.cgd.0c00589.

[24] I. Ben Shir, S. Kababya, I. Katz, B. Pokroy, A Schmidt, Exposed and buried biomineral interfaces in the aragonitic shell of Perna canaliculus revealed by Solid-State NMR, Chem. Mater. 25 (22) (2013) 4595–4602, https://doi.org/10.1021/cm4028226.

[25] V.K. Yadav, K.K. Yadav, M. Cabral-Pinto, N. Choudhary, G. Gnanamoorthy, V. Tirth, et al., The processing of calcium rich agricultural and industrial waste for recovery of calcium carbonate and calcium oxide and their application for environmental cleanup: a review, Appl. Sci. 11 (9) (2021) 4212, https://doi.org/10.3390/app11094212.

[26] K.L. Pickering, M.G.A. Efendy, T.M. Le, A review of recent developments in natural fibre composites and their mechanical performance, Compos. Part. A: Appl. Sci. Manuf. 83 (1) (2016) 98–112, https://doi.org/10.1016/j.compositesa.2015.08.038.

[27] O. Ersoy, H. Köse, Comparison of the effect of reactive and nonreactive treatments on the dispersion characteristics of a calcium carbonate (calcite) filler in a polypropylene matrix composite, Polym. Compos. 41 (9) (2020) 3483–3490, https://doi.org/10.1002/pc.25634.

[28] I. Acar, O. Acisli, Mechano-chemical surface modification of calcite by wet-stirred ball milling, Appl. Surf. Sci. 457 (2018) 208–213, https://doi.org/10.1016/j.apsusc.2018.06.247.

[29] M.E. Xanthos, Functional Fillers For Plastics, 2nd ed, WILEY-VCH Verlag GmbH & Co. KGaA, Weinheim, 2010.

[30] J. Lee, S.H. Jo, J. Lim, Effect of surface modification of CaCO3 nanoparticles by a silane coupling agent methyltrimethoxysilane on the stability of foam and emulsion, J. Ind. Eng. Chem. 74 (2019) 63–70, https://doi.org/10.1016/j.jiec.2019.02.002.

[31] E. Pérez, V. Alvarez, C.J. Pérez, C. Bernal, A comparative study of the effect of different rigid fillers on the fracture and failure behavior of polypropylene based composites, Composit. Part. B: Eng. 52 (2013) 72–83, https://doi.org/10.1016/j.compositesb.2013.03.035.

[32] Z.T. Yao, T. Chen, H.Y. Li, M.S. Xia, Y. Ye, H. Zheng, Mechanical and thermal properties of polypropylene (PP) composites filled with modified shell waste, J. Hazard. Mater. 262 (15) (2013) 212–217, https://doi.org/10.1016/j.jhazmat.2013.08.062.

[33] L.Q. Ge, W.Y. Yang, H. Lv, M.S. Xia, X.S. Ji, Z.T. Yao, Colorating and mechanical performance of low-density polyethylene (LDPE)/dye-loaded shell powder (DPSP) composites, Fiber. Polym. 16 (6) (2015) 1294–1302, https://doi.org/10.1007/s12221-015-1294-0.

[34] O.J. Gbadeyan, S. Adali, G. Bright, B. Sithole, S. Onwubu, Optimization of milling procedures for synthesizing nano-CaCO3 from Achatina fulica shell through mechanochemical techniques, J. Nanomater. 2020 (4) (2020) 1–9, https://doi.org/10.1155/2020/4370172.

[35] H. Hemmatpour, O. De Luca, D. Crestani, M.C.A. Stuart, A. Lasorsa, P.C.A. van der Wel, et al., New insights in polydopamine formation via surface adsorption, Nat. Commun. 14 (1) (2023) 664, https://doi.org/10.1038/s41467-023-36303-8.

[36] H. Lee, S.M. Dellatore, W.M. Miller, P.B. Messersmith, Mussel-inspired surface chemistry for multifunctional coatings, Science 318 (5849) (2007) 426–430, https://doi.org/10.1126/science.1147241.

[37] C.Y. Li, Z.J. Qian, C.X. Zhou, W.M. Su, P.Z. Hong, S.C. Liu, et al., Mussel-inspired synthesis of polydopamine-functionalized calcium carbonate as reusable adsorbents for heavy metal ions, RSC Adv. 4 (88) (2014) 47848–47852, https://doi.org/10.1039/c4ra08193e.

[38] L. Shanmugam, X. Feng, J Yang, Enhanced interphase between thermoplastic matrix and UHMWPE fiber sized with CNT-modified polydopamine coating, Compos. Sci. Tech. 174 (12) (2019) 212–220, https://doi.org/10.1016/j.compscitech.2019.03.001.

[39] K.L. Koh, X. Ji, A. Dasari, X. Lu, S.K. Lau, Z Chen, Fracture toughness and elastic modulus of epoxy-based nanocomposites with dopamine-modified aano-fillers, Mater. (Basel) 10 (7) (2017) 776, https://doi.org/10.3390/ma10070776.

[40] Y. Liu, Y. Fang, J. Qian, Z. Liu, B. Yang, X Wang, Bio-inspired polydopamine functionalization of carbon fiber for improving the interfacial adhesion of polypropylene composites, RSC Adv. 5 (130) (2015) 107652–107661, https://doi.org/10.1039/c5ra20045h.

[41] Y. Song, Y. Shen, H. Liu, Y. Lin, M. Li, C.-W. Nan, Improving the dielectric constants and breakdown strength of polymer composites: effects of the shape of the $BaTiO_3$ nanoinclusions, surface modification and polymer matrix, J. Mater. Chem. 22 (32) (2012) 16491–16498, https://doi.org/10.1039/C2JM32579A.

[42] G. Wang, X. Huang, P. Jiang, Tailoring dielectric properties and energy density of ferroelectric polymer nanocomposites by high-k nanowires, ACS Appl. Mater. Interface. 7 (32) (2015) 18017–18027, https://doi.org/10.1021/acsami.5b06480.

[43] ASTM-D790-17, Flexural Properties of Unreinforced and Reinforced Plastics and Electrical Insulating Materials, ASTM International, West Conshohocken, 2017.

[44] N.V. Vagenas, A. Gatsouli, C.G. Kontoyannis, Quantitative analysis of synthetic calcium carbonate polymorphs using FT-IR spectroscopy, Talanta 59 (4) (2003) 831–836, https://doi.org/10.1016/S0039-9140(02)00638-0.

[45] Y. Zhu, C. Sun, Y. Song, F. Jiang, X. Yin, M. Tang, et al., The study of the adductor muscle-shell interface structure in three Mollusc species, Acta Oceanolog. Sinica. 35 (8) (2016) 57–64, https://doi.org/10.1007/s13131-016-0878-x.

[46] S.W. Lee, Y.N. Jang, J.C. Kim, Characteristics of the aragonitic layer in adult oyster shells, Crassostrea gigas: structural study of Myostracum including the adductor muscle scar, J. Evid. Based Complement. Altern. Med. 2011 (1) (2011) 742963, https://doi.org/10.1155/2011/742963.

[47] H. Essabir, M.O. Bensalah, D. Rodrigue, R. Bouhfid, Qaiss Aek, A comparison between bio- and mineral calcium carbonate on the properties of polypropylene composites, Constr. Build. Mater. 134 (1) (2017) 549–555, https://doi.org/10.1016/j.conbuildmat.2016.12.199.

[48] H.Y. Li, Y.Q. Tan, L. Zhang, Y.X. Zhang, Y.H. Song, Y. Ye, et al., Bio-filler from waste shellfish shell: preparation, characterization, and its effect on the mechanical properties on polypropylene composites, J. Hazard. Mater. 217-218 (30) (2012) 256–262, https://doi.org/10.1016/j.jhazmat.2012.03.028.

[49] H. Nebel, M. Neumann, C. Mayer, M. Epple, On the structure of amorphous calcium carbonate-a detailed study by Solid-State NMR spectroscopy, Inorg. Chem. 47 (17) (2008) 7874–7879, https://doi.org/10.1021/ic8007409.

[50] C. Jäger, H. Cölfen, Fine structure of nacre revealed by solid state 13C and 1H NMR, Cryst. Eng. Comm. 9 (12) (2007) 1237, https://doi.org/10.1039/b708600h.

[51] S.Y. Fu, X.Q. Feng, B. Lauke, Y.W. Mai, Effects of particle size, particle/matrix interface adhesion and particle loading on mechanical properties of particulate–polymer composites, Compos. Part. B. Eng. 39 (6) (2008) 933–961, https://doi.org/10.1016/j.compositesb.2008.01.002.

[52] M. Ni, B.D. Ratner, Differentiating calcium carbonate polymorphs by surface analysis techniques-an XPS and TOF-SIMS study, SIA 40 (10) (2008) 1356–1361, https://doi.org/10.1002/sia.2904.

[53] Y. Xie, P.M. Sherwood, X-ray photoelectron-spectroscopic studies of carbon fiber surfaces. 11. Differences in the surface chemistry and bulk structure of different carbon fibers based on poly (acrylonitrile) and pitch and comparison with various graphite samples, Chem. Mater. 2 (3) (1990) 293–299, https://doi.org/10.1021/cm00009a020.

[54] A. Alkhouzaam, H. Qiblawey, M. Khraisheh, Polydopamine functionalized graphene oxide as membrane nanofiller: spectral and structural studies, Membranes 11 (2) (2021) 86, https://doi.org/10.3390/membranes11020086.

[55] X. Zhou, W. Liu, C. Tian, S. Mo, X. Liu, H. Deng, et al., Mussel-inspired functionalization of biological calcium carbonate for improving Eu(III) adsorption

and the related mechanisms, J. Chem. Eng. 351 (1) (2018) 816–824, https://doi.org/10.1016/j.cej.2018.06.142.
[56] F.Y. Gong, J.H. Zhang, L. Ding, Z.J. Yang, X.B. Liu, Mussel-inspired coating of energetic crystals: a compact core–shell structure with highly enhanced thermal stability, J. Chem. Eng. 309 (1) (2017) 140–150, https://doi.org/10.1016/j.cej.2016.10.020.
[57] J. Liebscher, R. Mrówczyński, H.A. Scheidt, C. Filip, N.D. Hădade, R. Turcu, et al., Structure of polydopamine: a never-ending story? Langmuir 29 (33) (2013) 10539–10548, https://doi.org/10.1021/la4020288.
[58] K. Stöckelhuber, S. Wießner, A. Das, G. Heinrich, Filler flocculation in polymers–a simplified model derived from thermodynamics and game theory, J. Soft. Matter. 13 (20) (2017) 3701–3709, https://doi.org/10.1039/C6SM02694J.
[59] A. Taguet, P. Cassagnau, J.M. Lopez-Cuesta, Structuration, selective dispersion and compatibilizing effect of (nano)fillers in polymer blends, Prog. Polym. Sci. 39 (8) (2014) 1526–1563, https://doi.org/10.1016/j.progpolymsci.2014.04.002.
[60] C. Lin, F. Gong, W. Qian, X. Huang, X. Tu, Sun Ga, et al., Tunable interfacial interaction intensity: construction of a bio-inspired interface between polydopamine and energetic crystals, Compos. Sci. Technol. 211 (28) (2021) 108816, https://doi.org/10.1016/j.compscitech.2021.108816.
[61] Q. Ma, Z. Wang, T. Liang, Y. Su, J. Li, Y. Yao, et al., Unveiling the role of filler surface energy in enhancing thermal conductivity and mechanical properties of thermal interface materials, Compos. Part. A: Appl. Sci. Manuf. 157 (1) (2022) 106904, https://doi.org/10.1016/j.compositesa.2022.106904.
[62] V. Khoshkava, M.R. Kamal, Effect of surface energy on dispersion and mechanical properties of polymer/nanocrystalline cellulose nanocomposites, Biomacromolecules 14 (9) (2013) 3155–3163, https://doi.org/10.1021/bm400784j.
[63] S.M. Mirabedini, H. Rahimi, S. Hamedifar, S. Mohsen Mohseni, Microwave irradiation of polypropylene surface: a study on wettability and adhesion, Int. J. Adhes. Adhes. 24 (2) (2004) 163–170, https://doi.org/10.1016/j.ijadhadh.2003.09.004.
[64] F.M. Fowkes, Additivity of intermolecular forces at interfaces. I. determination of the contribution to surface and interfacial tensions of dispersion forces in various liquids1, J. Phys. Chem. 67 (12) (1963) 2538–2541, https://doi.org/10.1021/j100806a008.
[65] B. Natarajan, Y. Li, H. Deng, L.C. Brinson, L.S. Schadler, Effect of interfacial energetics on dispersion and glass transition temperature in polymer nanocomposites, Macromol. 46 (7) (2013) 2833–2841, https://doi.org/10.1021/ma302281b.
[66] M.J. Wang, Effect of polymer-filler and filler-filler interactions on dynamic properties of filled vulcanizates, Rubb. Chem. Tech. 71 (3) (1998) 520–589, https://doi.org/10.5254/1.3538492.
[67] H.S. Kim, B.H. Lee, S.W. Choi, S. Kim, H.J. Kim, The effect of types of maleic anhydride-grafted polypropylene (MAPP) on the interfacial adhesion properties of bio-flour-filled polypropylene composites, Compos. Part. A: Appl. Sci. Manuf. 38 (6) (2007) 1473–1482, https://doi.org/10.1016/j.compositesa.2007.01.004.
[68] J.Z. Lu, Q. Wu, I.I. Negulescu, Wood-fiber/high-density-polyethylene composites: coupling agent performance, J. Appl. Polym. Sci. 96 (1) (2005) 93–102, https://doi.org/10.1002/app.21410.
[69] S. Niwa, T. Ogawa, S. Ogoe, Y. Teramoto, Wetting and localization of compatibilizers in biocomposites: a nanoscale evaluation and effects on physical properties, Polymer. (Guildf). 185 (17) (2019) 121963, https://doi.org/10.1016/j.polymer.2019.121963.
[70] V. Ambrogi, G. Gentile, C. Ducati, M.C. Oliva, C. Carfagna, Multiwalled carbon nanotubes functionalized with maleated poly(propylene) by a dry mechano-chemical process, Polym. (Guildf.) 53 (2) (2012) 291–299, https://doi.org/10.1016/j.polymer.2011.11.048.
[71] W. Qiu, T. Endo, T. Hirotsu, Interfacial interactions of a novel mechanochemical composite of cellulose with maleated polypropylene, J. Appl. Polym. Sci. 94 (3) (2004) 1326–1335, https://doi.org/10.1002/app.21123.
[72] I.L. Dubnikova, V.G. Oshmyan, Y.G A, Mechanisms of particulate filled polypropylene finite plastic deformation and fracture, J. Mater. Sci. 32 (6) (1997) 1613–1622, https://doi.org/10.1023/A:1018547226983.
[73] C. Echeverria, F. Pahlevani, V. Gaikwad, V. Sahajwalla, The effect of microstructure, filler load and surface adhesion of marine bio-fillers, in the performance of Hybrid Wood-Polypropylene Particulate Bio-composite, J. Clean. Prod. 154 (1) (2017) 284–294, https://doi.org/10.1016/j.jclepro.2017.04.020.